On the inviscid instability of the hyperbolic-tangent velocity profile

By A. MICHALKE

DVL-Institut für Turbulenzforschung, Berlin

(Received 14 January 1964)

The Rayleigh stability equation of inviscid linearized stability theory was integrated numerically for amplified disturbances of the hyperbolic-tangent velocity profile. The evaluation of the eigenvalues and eigenfunctions is followed by a discussion of the streamline pattern of the disturbed flow. Here no qualitative distinction is found between an amplified and the neutral disturbance. But considering the vorticity distribution of the disturbed flow it is shown that in the case of amplified disturbances two concentrations of vorticity occur within a disturbance wavelength, while in the neutral case only one maximum of vorticity exists. The results are discussed with respect to the instability mechanism of free boundary-layer flow.

1. Introduction

It is well-known that two-dimensional unidirectional flow of an inviscid fluid cannot be unstable with respect to small wavy disturbances unless the velocity profile has an inflexion point. This theorem was first formulated by Rayleigh (1880). Later Tollmien (1935) showed that in certain circumstances the existence of an inflexion point is a sufficient condition for instability. A special class of profiles with inflexion points is provided by jets and wakes. They also have a certain importance in meteorology in connexion with the formation of cyclones.

The instability mechanism of such velocity profiles is an inviscid one, and the presence of viscosity will only damp this process. Velocity profiles without an inflexion point, e.g. the boundary-layer profiles of a flat plate, are stable without viscosity, and an instability can occur only if viscosity is taken into account (Lin 1955). Stability calculations by Lessen (1950) and Esch (1957) for special free boundary-layer profiles taking viscosity into account have shown actually that for large Reynolds numbers the neutral curve approaches asymptotically the inviscid value. The same result was obtained by Tatsumi & Kakutani (1958) who dealt with the instability of a plane jet. This was also confirmed by experimental investigations of plane and axisymmetric jets by Sato (1960), Schade & Michalke (1962) and Wille (1963). Thus for large Reynolds numbers it is sufficient to calculate the instability of free boundary layers neglecting the viscosity.

Furthermore, for small viscosity the velocity component v perpendicular to the basic flow is small compared with the u-component. The flow can then be considered approximately parallel and the linearized stability theory of parallel flow is applicable to the instability of boundary-layer velocity profiles.

The simplest case of a velocity profile with an inflexion point consists of two streams of different but constant velocities separated by a surface of discontinuity. Helmholtz (1868) has shown that this 'jump'-profile is unstable. Rayleigh (1880) has considered the shear layer of finite thickness in which the velocity decreases linearly from a maximum value to zero. For this 'broken-line' profile he calculated the growth rate of amplified disturbances as a function of the disturbance wave-number in closed form. For special steadily curved half-jet profiles the inviscid stability characteristics were calculated by Carrier (1954) and by Lessen & Fox (1955). In the case of the analytically very simple hyperbolic-tangent velocity profile the eigenvalue and the eigenfunction of the neutral disturbance were given by Garcia (1956). For small wave-numbers of the disturbance the instability characteristics of this profile were calculated by Drazin & Howard (1962).

As a contribution to the understanding of the instability mechanism of free boundary layers at infinite Reynolds numbers this paper presents the results of a numerical computation of the eigenvalues and the eigenfunctions of the Rayleigh stability equation as well as the streamlines and the vorticity distribution of the disturbed hyperbolic-tangent profile.

2. The inviscid linearized disturbance equation in the two-dimensional case

Rayleigh (1880) derived, for the two-dimensional case, the differential equation of a small disturbance in an inviscid flow with a basic velocity $U(y)$ in the x-direction. A small disturbance $u_1(x,y,t)$ and $v_1(x,y,t)$ is superimposed on the basic flow with the assumption $u_1 \ll U$ and $v_1 \ll U$. A stream function $\psi_1(x,y,t)$ for the disturbance motion is defined by

$$u_1 = \partial\psi_1/\partial y, \quad v_1 = -\partial\psi_1/\partial x. \tag{1}$$

Furthermore, we consider a wavy disturbance and write the stream function as

$$\psi_1(x,y,t) = \mathscr{R}[\phi(y)\, e^{i\alpha(x-ct)}], \tag{2}$$

where $\phi(y)$ is the amplitude and α the wave-number of the disturbance. The quantity $c = c_r + ic_i$ is generally complex; c_r is the phase velocity and c_i a measure of the amplification of the disturbance.† Inserting (1) and (2) into the Euler equation of motion and neglecting the second-order terms of the disturbance we obtain the Rayleigh stability equation

$$[U-c][\phi''-\alpha^2\phi]-U''\phi = 0, \tag{3}$$

where primes denote differentiation with respect to y.

For unbounded velocity profiles the disturbance must vanish at infinity, so the boundary conditions are

$$\phi(-\infty) = \phi(+\infty) = 0. \tag{4}$$

† Formally the amplification or damping of a disturbance seems to depend on whether c_i is greater or smaller than zero. But Lin (1955) has shown that results of inviscid stability theory are physically only significant for amplified disturbances.

We therefore have to solve an eigenvalue problem in order to determine $c = c(\alpha)$. Since c is generally complex, $\phi = \phi_r + i\phi_i$ will be complex too. The behaviour of unbounded velocity profiles for large values of y is determined by the condition

$$\lim_{y \to \pm\infty} U''(y) = 0. \tag{5}$$

Thus for the asymptotic behaviour of the eigenfunctions ϕ it follows from (3), if the boundary condition (4) is to be satisfied, that for $y \to +\infty$

$$\phi \sim e^{-\alpha y}, \quad \phi' \sim -\alpha\phi, \tag{6}$$

and for $y \to -\infty$

$$\phi \sim e^{\alpha y}, \quad \phi' \sim \alpha\phi. \tag{7}$$

To simplify the numerical evaluation of the eigenvalues we set

$$\phi \sim \exp\left(\int \Phi\, dy\right). \tag{8}$$

Thus we obtain from (3) the corresponding Riccati equation in $\Phi(y)$:

$$\Phi' = \alpha^2 - \Phi^2 + U''/(U-c). \tag{9}$$

The boundary conditions for $\Phi(y)$ become, according to (6) and (7),

$$\Phi(+\infty) = -\alpha, \quad \Phi(-\infty) = +\alpha. \tag{10}$$

3. Evaluation of the eigenvalues for the hyperbolic-tangent profile

The velocity profile whose stability is investigated here is given in dimensionless form by

$$U(y) = 0{\cdot}5[1 + \tanh y] \tag{11}$$

and shown in figure 1. Since the profile is antisymmetric with respect to its inflexion point ($y = 0$), it follows (Tatsumi & Gotoh 1960) that, provided the unstable eigenfunction is unique, the phase velocity c_r of the disturbance is independent of the wave-number α, and

$$c_r = U(0) = 0{\cdot}5. \tag{12}$$

In the neutral case we have $c_i = 0$. Then equation (3) can be written

$$\phi'' - [\alpha^2 - 2(1 - \tanh^2 y)]\,\phi = 0. \tag{13}$$

The symmetric and antisymmetric solutions of (13) are

$$\left.\begin{aligned} \phi_1 &= \alpha \cosh \alpha y - \sinh \alpha y \tanh y, \\ \phi_2 &= \alpha \sinh \alpha y - \cosh \alpha y \tanh y. \end{aligned}\right\} \tag{14}$$

The only eigenvalue is $\alpha = 1$. Then the eigenfunction is

$$\phi = \phi_1 = \operatorname{sech} y, \tag{15}$$

which was given by Garcia (1956)

In order to evaluate the eigenvalues $c_i \neq 0$, the differential equation (9) must be integrated numerically. But first the new independent variable

$$z = \tanh y \tag{16}$$

is introduced in order to reduce the integration region to a finite interval. Then we obtain using (11) and (12)

$$\frac{d\Phi}{dz} = \frac{\alpha^2 - \Phi^2}{1-z^2} - \frac{2z}{z - i2c_i}. \tag{17}$$

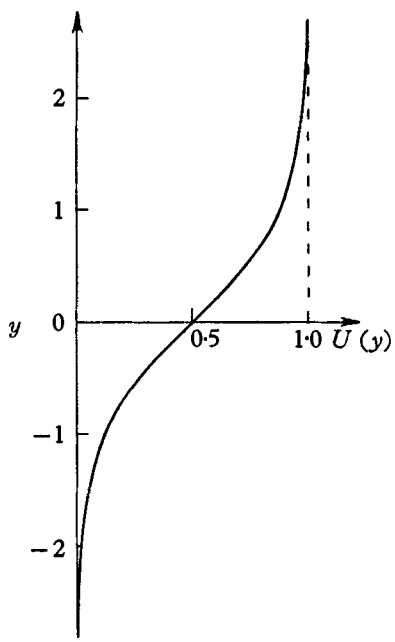

FIGURE 1. Hyperbolic-tangent velocity profile.

Separating the real and imaginary part, $\Phi = \Phi_r + i\Phi_i$, we get the following system of differential equations of first order:

$$\left.\begin{aligned} \frac{d\Phi_r}{dz} &= \frac{\alpha^2 - \Phi_r^2 + \Phi_i^2}{1-z^2} - \frac{2z^2}{z^2 + (2c_i)^2}, \\ \frac{d\Phi_i}{dz} &= -\frac{2\Phi_r\Phi_i}{1-z^2} - \frac{4c_i z}{z^2 + (2c_i)^2}. \end{aligned}\right\} \tag{18}$$

The transformed boundary conditions are

$$\left.\begin{aligned} &\Phi_r(1) = -\alpha, \quad \Phi_r(-1) = +\alpha; \\ &\Phi_i(1) = 0, \quad \Phi_i(-1) = 0. \end{aligned}\right\} \tag{19}$$

At the boundaries $z = \pm 1$ the derivatives of $\Phi(z)$ are undetermined. But using L'Hospital's rule we can evaluate the limiting values from (18). They are

$$\left.\begin{aligned} \left.\frac{d\Phi_r}{dz}\right|_{z=1} &= -\frac{2}{[1+(2c_i)^2](\alpha+1)}, & \left.\frac{d\Phi_r}{dz}\right|_{z=-1} &= -\frac{2}{[1+(2c_i)^2](\alpha+1)}; \\ \left.\frac{d\Phi_i}{dz}\right|_{z=1} &= -\frac{4c_i}{[1+(2c_i)^2](\alpha+1)}, & \left.\frac{d\Phi_i}{dz}\right|_{z=-1} &= \frac{4c_i}{[1+(2c_i)^2](\alpha+1)}. \end{aligned}\right\} \tag{20}$$

As can be seen from equations (18), $\Phi_r(z)$ must be an antisymmetric function and $\Phi_i(z)$ a symmetric one. Therefore it is sufficient to integrate (18) in the interval $-1 \leqq z \leqq 0$. Equations (18) were integrated numerically for fixed wave-number α starting from $z = -1$ with the initial condition (19) and with reference to (20), choosing c_i by trial and error so that

$$\Phi_r(0) = 0, \quad (d\Phi_i/dz)_{z=0} = 0. \tag{21}$$

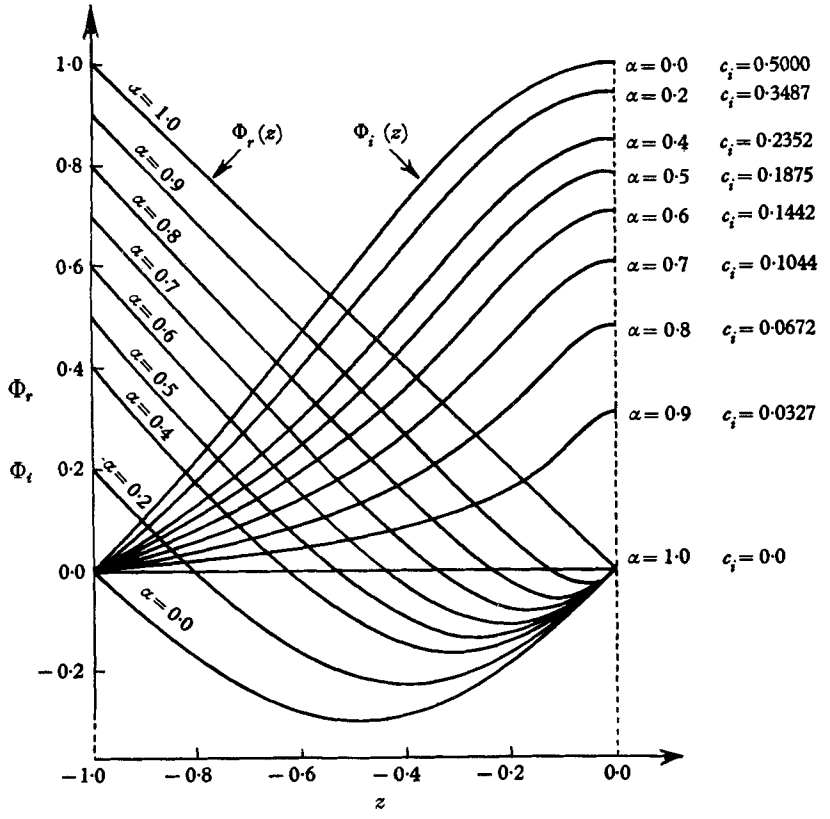

FIGURE 2. Solutions $\Phi(z)$ of equation (18) for various wave-numbers α.

The integration was performed on a LGP 30 digital computer using a Runge–Kutta procedure with an integration step of $\Delta z = 0{\cdot}025$.

For the 'trivial' cases $\alpha = 1$ and $\alpha = 0$ the functions $\Phi(z)$ can be written down in closed form. They become

$$\text{for } \alpha = 1: \qquad \Phi_r(z) = -z, \quad \Phi_i(z) \equiv 0; \tag{22}$$

$$\text{and for } \alpha = 0: \qquad \Phi_r(z) = \frac{z(1-z^2)}{z^2+(2c_i)^2}, \quad \Phi_i(z) = \frac{2c_i(1-z^2)}{z^2+(2c_i)^2}. \tag{23}$$

The latter function satisfies the boundary conditions (19) for any c_i, i.e. the solution is not unique. But from the solutions for $\alpha \to 0$, we find that we have to choose $c_i = 0{\cdot}5$.

Some functions $\Phi(z)$ are plotted in figure 2. The eigenvalues c_i are given in table 1 and plotted *vs* the wave-number α in figure 3. For small values of α the

results are compared with the values from the 3-term approximation by Drazin & Howard (1962). Up to the wave-number $\alpha = 0{\cdot}2$ the agreement is good. The growth rate αc_i as a function of the wave-number α is also plotted in figure 3. The maximum amplification is $\alpha c_{i\,\max} = 0{\cdot}0949$ and occurs at $\alpha = 0{\cdot}4446$.

α	c_i	αc_i
1·0000	0·0000	0·00000
0·9000	0·0327	0·02942
0·8000	0·0674	0·05388
0·7000	0·1044	0·07305
0·6000	0·1442	0·08650
0·5000	0·1875	0·09376
0·4000	0·2352	0·09410
0·3000	0·2885	0·08654
0·2000	0·3487	0·06975
0·1000	0·4184	0·04184
0·0000	0·5000	0·00000
0·4446	0·2133	0·09485

TABLE 1

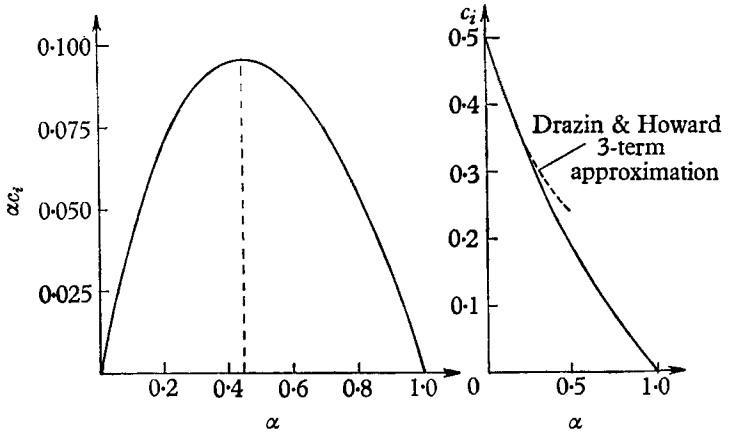

FIGURE 3. Eigenvalues c_i and growth rate αc_i *vs* wave-number α of the hyperbolic-tangent velocity profile.

4. Evaluation of the eigenfunctions for the hyperbolic-tangent profile

With the computed eigenvalues we can now evaluate the eigenfunctions of the Rayleigh stability equation by integrating (3). From (8) it follows that $\phi_r(y)$ is a symmetric function and $\phi_i(y)$ an antisymmetric one. Therefore we can restrict the integration to the interval $0 \leqq y < \infty$. Since the eigenfunctions are determined except for an arbitrary multiplicative constant alone, we normalize the initial values conveniently to

$$\phi_r(0) = 1, \quad \phi_i(0) = 0. \tag{24}$$

The initial gradient is given by (8),

$$\phi'(0) = \Phi(0)\,\phi(0), \tag{25}$$

or

$$\phi_r'(0) = 0, \quad \phi_i'(0) = \Phi_i(0). \tag{26}$$

$\Phi_i(0)$, however, is known from the evaluation of the eigenvalues (§3). With the initial values (24) and (26) the Rayleigh stability equation (3) was now solved using a Runge–Kutta procedure. In figures 4 and 5 the eigenfunctions $\phi_r(y)$ and $\phi_i(y)$ are shown for the wave-numbers $\alpha = 1$, $\alpha = 0{\cdot}9$, $\alpha = 0{\cdot}6$, $\alpha = 0{\cdot}4446$, $\alpha = 0{\cdot}2$ and $\alpha = 0$. For the 'trivial' case $\alpha = 0$ the eigenfunctions are

$$\phi_r(y) \equiv 1, \quad \phi_i(y) = \tanh y. \tag{27}$$

It should be noticed that at $y = 0$ we have, for all wave-numbers $0 < \alpha < 1$,

$$\phi_r''(0) = \alpha^2 \phi_r(0) > 0. \tag{28}$$

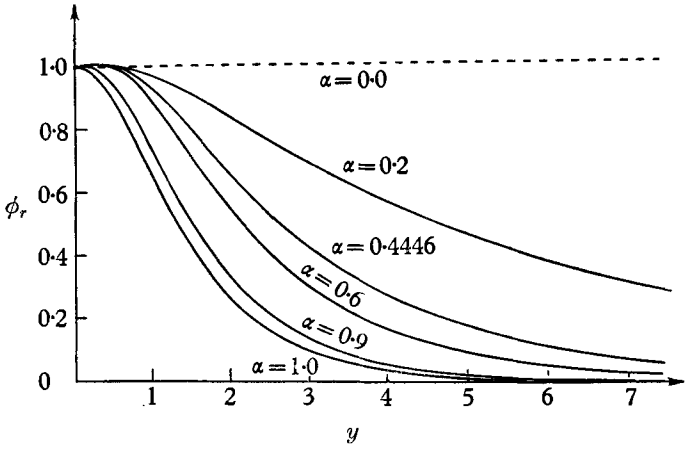

FIGURE 4. Eigenfunctions $\phi_r(y)$ of the hyperbolic-tangent velocity profile for various wave-numbers α.

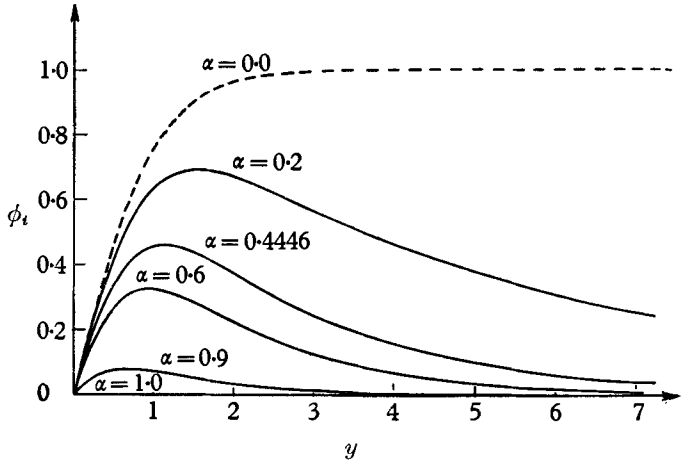

FIGURE 5. Eigenfunctions $\phi_i(y)$ of the hyperbolic-tangent velocity profile for various wave-numbers α.

5. Streamlines of the disturbed hyperbolic-tangent profile

Knowing the solution of the Rayleigh stability equation, let us now consider the physical properties of the disturbed tanh profile. First, it may be of interest to calculate the stream function $\psi(x, y, t)$ and especially the streamlines $\psi = \text{const.}$ of the disturbed flow. This stream function is found by adding the stream

function $\psi_1(x, y, t)$ of the disturbance to the stream function $\psi_0(y)$ of the basic flow. In our case we have

$$\psi_0 = \int U\,dy + \text{const.} = y + \tfrac{1}{2}\ln(1+e^{-2y}), \tag{29}$$

where the constant is determined by the condition $\psi_0(-\infty) = 0$. Further, the disturbance stream function becomes with (2)

$$\psi_1(x, y, t) = e^{\alpha c_i t}[\phi_r(y)\cos\alpha(x - c_r t) - \phi_i(y)\sin\alpha(x - c_r t)]. \tag{30}$$

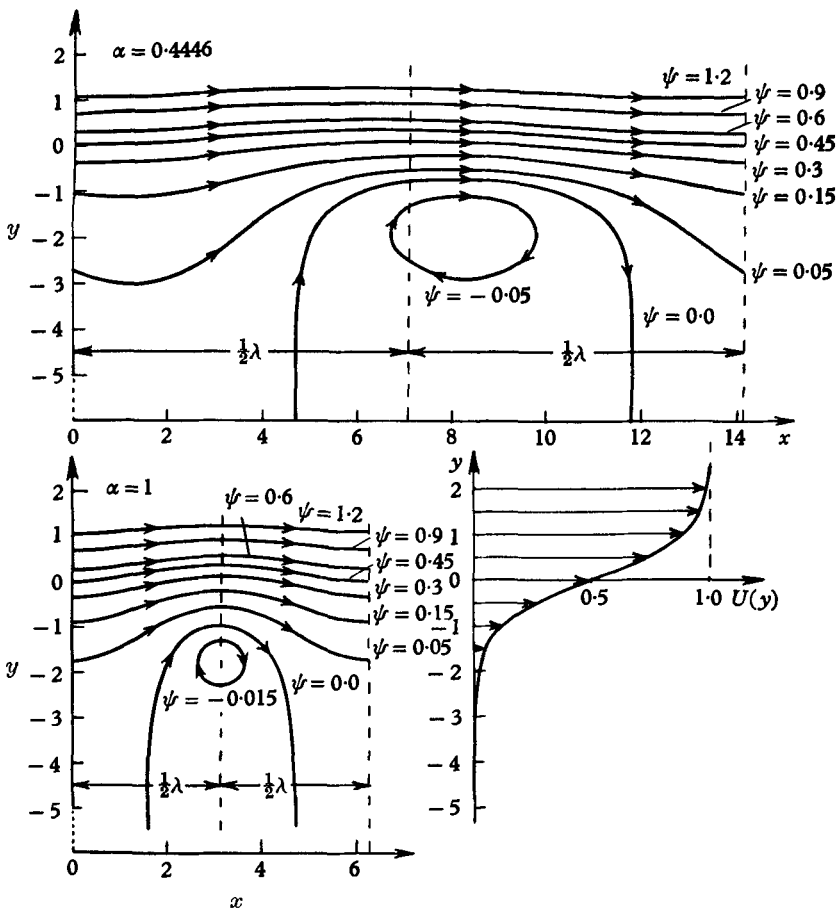

FIGURE 6. Streamlines of the disturbed velocity profile $U(y) = 0{\cdot}5[1 + \tanh y]$ for the wave-numbers of maximum amplification $\alpha = 0{\cdot}4446$ and of the neutral disturbance $\alpha = 1$ at the time $t = 0$ and a disturbance magnitude $\epsilon = 0{\cdot}1$.

The total stream function is given by

$$\psi(x, y, t) = \psi_0 + \epsilon\psi_1 = y + \tfrac{1}{2}\ln(1+e^{-2y}) + \epsilon e^{\alpha c_i t}[\phi_r(y)\cos\alpha(x - c_r t) - \phi_i(y)\sin\alpha(x - c_r t)], \tag{31}$$

where ϵ is an arbitrary constant which may be interpreted as a measure of the magnitude of the disturbance. Small disturbances are present if $\epsilon \ll 1$. The stream-

lines $\psi = \text{const.}$ depend on the time t. But without loss of generality we can put $t = 0$ in order to study the behaviour of the disturbed flow. The streamlines

$$\psi = y + \tfrac{1}{2}\ln(1+e^{-2y}) + \epsilon[\phi_r(y)\cos\alpha x - \phi_i(y)\sin\alpha x] = \text{const.} \tag{32}$$

were computed numerically using an iteration process. They are shown in figure 6 for the most strongly amplified wave-number $\alpha = 0{\cdot}4446$ and for the neutral case $\alpha = 1$ assuming $\epsilon = 0{\cdot}1$. Qualitatively there seems to be no distinction

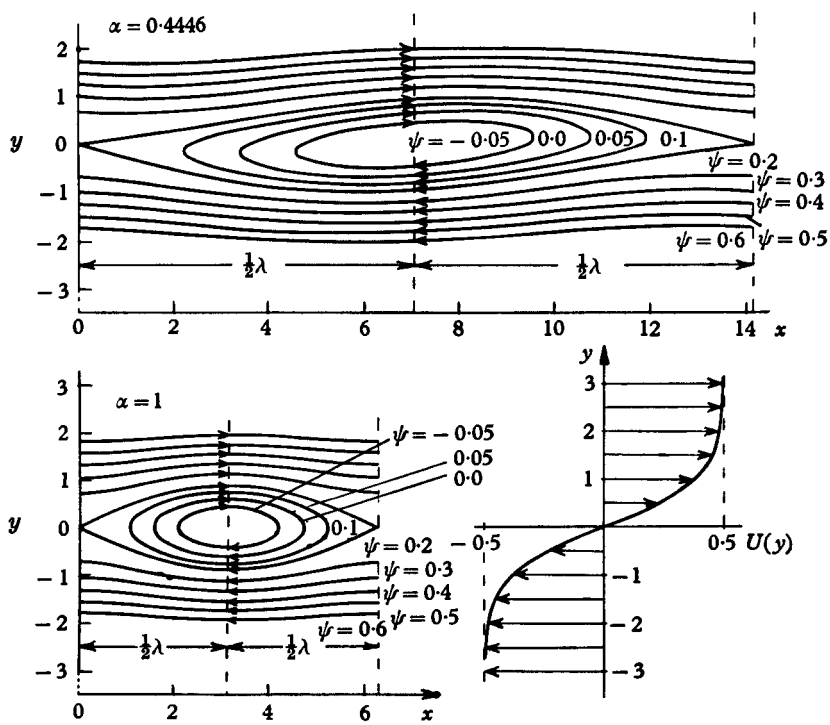

FIGURE 7. Streamlines of the disturbed velocity profile $U(y) = 0{\cdot}5\tanh y$ for the wave-numbers of maximum amplification $\alpha = 0{\cdot}4446$ and of the neutral disturbance $\alpha = 1$ at the time $t = 0$ and a disturbance magnitude $\epsilon = 0{\cdot}1$.

between the streamline pattern of the most strongly amplified and the neutral disturbance. The streamlines of the basic flow, which are straight lines parallel to the x-axis, are displaced wavily by the disturbance. The amplitude of this displacement is large in the range of small velocities ($y < 0$) and decreases with increasing velocity ($y > 0$). Furthermore, there exists a region of rotating fluid in the range of small velocity. A quantitative comparison between the neutral and the most strongly amplified disturbance shows that the centre of the rotating fluid region within a wavelength λ is shifted downstream for $\alpha = 0{\cdot}4446$ unlike the situation for $\alpha = 1$.

Another shape of the streamline pattern is obtained, when we move downstream with the phase velocity of the disturbance. Then the relative basic flow is described by the velocity profile

$$U(y) = 0{\cdot}5\tanh y \tag{33}$$

and the corresponding stream function is

$$\psi_0(y) = 0{\cdot}5 \ln(\cosh y). \tag{34}$$

The solution of the Rayleigh stability equation for the profile (33) differs from that for the profile (11) only by $c_r = 0$. Therefore the stream function for the profile (33) at the time $t = 0$ is

$$\psi = \tfrac{1}{2} \ln(\cosh y) + \epsilon[\phi_r(y) \cos \alpha x - \phi_i(y) \sin \alpha x]. \tag{35}$$

The streamlines $\psi = \text{const.}$ of this profile (33) are shown in figure 7 for the wave-number $\alpha = 0{\cdot}4446$ and $\alpha = 1$ and for $\epsilon = 0{\cdot}1$. In both cases now the rotating fluid regions occur at another part of the profile, namely in the neighbourhood of $y = 0$, where the velocity (33) of the basic flow becomes zero. One may suppose that the rotating fluid region may be produced by a 'vortex', i.e. by a concentration of vorticity, which is surely not a potential vortex. We cannot, however, conclude from figures 6 and 7 that the 'vortices' are placed at different positions for the profiles (11) and (33), because the rotating fluid-regions appear at different positions. This cannot be true, since the vorticity distribution is not changed when a constant velocity is superimposed on a velocity profile. Therefore, considering the rotating fluid regions, it cannot be decided whether and where a concentration of vorticity exists. Thus we see that no essential insight in the instability mechanism is gained from a study of the streamlines of the disturbed flow. This may be expected only by considering the vorticity distribution, as it was stated by Lin (1955).

6. Vorticity distribution of the disturbed hyperbolic-tangent profile

The distribution of vorticity Ω_0 of the basic flow is given by

$$\Omega_0 = -dU/dy = -\tfrac{1}{2} \operatorname{sech}^2 y \tag{36}$$

and is the same for both profiles (11) and (33). The vorticity of the disturbance becomes, from (1),

$$\Omega_1 = \partial v_1/\partial x - \partial u_1/\partial y = -\Delta \psi_1. \tag{37}$$

If we set

$$\Omega_1 = \mathscr{R}[\omega(y)\, e^{i\alpha(x-ct)}], \tag{38}$$

then using (2) and (3) the complex amplitude function $\omega(y)$ of the vorticity is obtained as

$$\omega(y) = -[\phi'' - \alpha^2 \phi] = -\{U''/(U-c)\}\phi, \tag{39}$$

where $\omega_r(y)$ is a symmetric function and $\omega_i(y)$ an antisymmetric one. The vorticity amplitude $\omega(y)$ according to (39) was computed together with the eigenfunctions (§4). For the neutral case, $\alpha = 1$, it follows that

$$\omega_r = 2 \operatorname{sech}^3 y, \quad \omega_i \equiv 0, \tag{40}$$

and, for $\alpha = 0$,

$$\omega_r \equiv 0, \quad \omega_i = 2 \tanh y \operatorname{sech}^2 y. \tag{41}$$

In figure 8 $\omega_r(y)$ and $\omega_i(y)$ are plotted for the wave-numbers $\alpha = 1$, $\alpha = 0{\cdot}9$, $\alpha = 0{\cdot}6$, $\alpha = 0{\cdot}4446$, $\alpha = 0{\cdot}2$ and $\alpha = 0$. From equation (39) we see that $\omega_r(0) = 0$ for $c_i \neq 0$ according to $U''(0) = 0$, but for $c_i = 0$ we have $\omega_r(0) = 2$. Therefore it is evident that there is no uniform convergence of $\omega_r(0)$ as $c_i \to 0$, and the gradient $d\omega_r/dy$ increases rapidly in the neighbourhood of $y = 0$ as $c_i \to 0$. This seems to be due to the neglect of viscosity.

The distribution of the disturbance vorticity (38) is given by

$$\Omega_1(x, y, t) = e^{\alpha c_i t}[\omega_r(y)\cos\alpha(x - c_r t) - \omega_i(y)\sin\alpha(x - c_r t)]. \tag{42}$$

This can be written as

$$\Omega_1 = (\omega_r^2 + \omega_i^2)^{\frac{1}{2}} e^{\alpha c_i t}\cos[\alpha(x - c_r t) + \chi(y)], \tag{43}$$

with the phase angle χ defined by

$$\tan\chi(y) = \omega_i(y)/\omega_r(y). \tag{44}$$

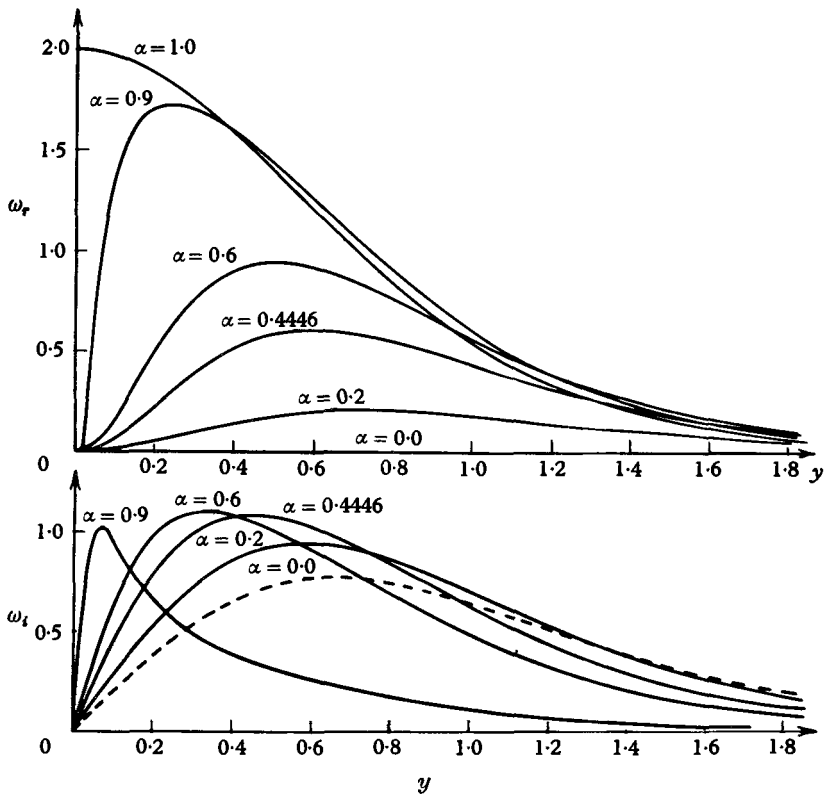

FIGURE 8. Vorticity amplitude $\omega_r(y)$ and $\omega_i(y)$ of the hyperbolic-tangent velocity profile for various wave-numbers α.

The wavy disturbance (2) which was assumed for the stability calculation can also be interpreted as a vorticity disturbance as Michalke (1963) showed for the Rayleigh shear layer. The magnitude of Ω_1 at $t = 0$,

$$|\Omega_1| = (\omega_r^2 + \omega_i^2)^{\frac{1}{2}}, \tag{45}$$

is plotted in figure 9. From (43) it can be seen that for $c_i \neq 0$ two maxima of vorticity with $\Omega_1 < 0$ exist outside the critical layer $y = 0$, one for $y < 0$ and one for $y > 0$ within a wavelength λ. Only one maximum with $\Omega_1 < 0$, however, is found for $c_i = 0$ within a wavelength λ, and that is at $x = \frac{1}{2}\lambda$, $y = 0$. Thus we see that there is a qualitative distinction between amplified disturbances and the neutral disturbance in the distribution of vorticity.

This distinction can be more clearly observed if we consider the total vorticity distribution, which is given by

$$\Omega = \Omega_0 + \epsilon\Omega_1 = -\tfrac{1}{2}\operatorname{sech}^2 y + \epsilon e^{\alpha c_i t}[\omega_r(y)\cos\alpha(x-c_r t) - \omega_i(y)\sin\alpha(x-c_r t)]. \quad (46)$$

For $t = 0$, the lines of constant vorticity were computed from the formula

$$\Omega = -\tfrac{1}{2}\operatorname{sech}^2 y + \epsilon[\omega_r(y)\cos\alpha x - \omega_i(y)\sin\alpha x] = \text{const.} \quad (47)$$

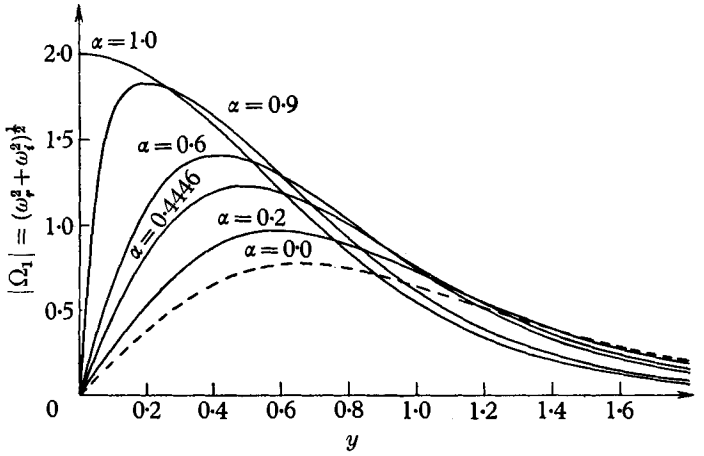

FIGURE 9. Magnitude $|\Omega_1|$ of the disturbance vorticity of the hyperbolic-tangent velocity profile for various wave-numbers α.

The results are plotted in figure 10 for $\alpha = 0{\cdot}4446$ and $\alpha = 1$, using the relatively large value 0·2 for ϵ in order to show the phenomenon more clearly. It is evident that for the most strongly amplified disturbance two maxima of vorticity are present within a wavelength, but only one maximum for the neutral disturbance, as indicated above.

If we interpret these concentrations of vorticity as 'vortices', it is obvious that in the neutral case the arrangement of vorticity corresponds essentially to a one-row vortex street. With respect to their mutual induction this arrangement is an equilibrium state of motion. Yet in the case of amplified disturbances the arrangement of vorticity corresponds to two parallel vortex rows which are displaced relative to one another. Therefore an equilibrium state exists no more. Both 'elementary vortices' within a wavelength will obviously have a tendency to rotate around their centre or, taking the transport velocity into account, to slip round each other. This behaviour has been explained by Domm (1956). We may expect that under the influence of viscosity the two 'elementary vortices' might coalesce. This process might then explain the formation of vortices in free boundary layers, which have been observed in experiments, among others by Schade & Michalke (1962) and Wille (1963). It was found that in the fully developed vortex flow of free boundary layers to consecutive vortices do 'slip' and, finally, coalesce into a vortex of larger intensity, if they are displaced relative to one another. A similar initial state obviously arises in the disturbed free boundary layer according to linearized stability theory, as mentioned above.

But these considerations go far beyond the framework of inviscid linearized stability theory. In order to prove this hypothesis about the formation of vortices in free boundary layers the non-linear development of the disturbed free boundary layer must be investigated, e.g. by application of the theory by Stuart (1961) and Watson (1960). A first attempt to calculate the non-linear development of the disturbed Rayleigh shear layer was made by Michalke (1963) using a very rough approximation.

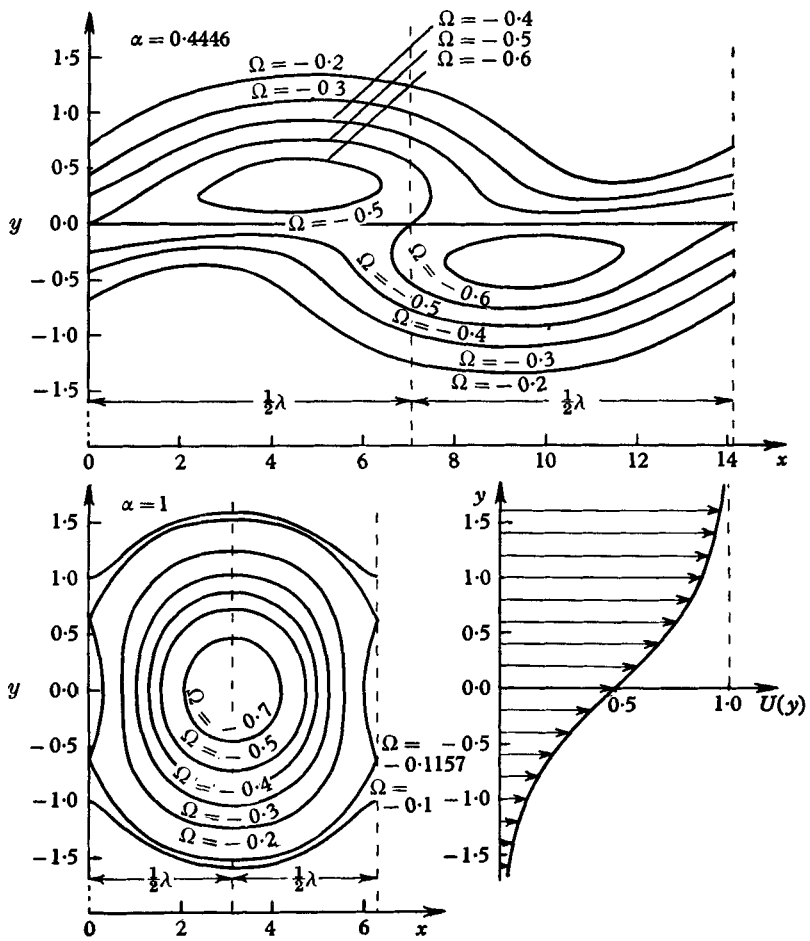

FIGURE 10. Lines of constant vorticity of the disturbed hyperbolic-tangent velocity profile for the wave-numbers of maximum amplification $\alpha = 0{\cdot}4446$ and of the neutral disturbance $\alpha = 1$ at the time $t = 0$ and a disturbance magnitude $\epsilon = 0{\cdot}2$.

This work was done at the Institut für Turbulenzforschung of the Deutsche Versuchsanstalt für Luft- und Raumfahrt e.V. at Berlin. The author wishes to express his thanks to Professor Dr.-Ing. R. Wille, the Director of the Institute, for his interest in this work. The author is also much indebted to Dr.-Ing. H. Schade for many stimulating discussions. The Deutsche Forschungsgemeinschaft, Bad Godesberg, kindly provided financially for the numerical computations.

REFERENCES

CARRIER, G. F. 1954 *Los Alamos Internal Rep.*

DOMM, U. 1956 *Deutsche Versuchsanstalt f.Luftfahrt, Porz-Wahn, DVL-Rep.* no. 26.

DRAZIN, P. G. & HOWARD, L. N. 1962 *J. Fluid Mech.* **14**, 257–83.

ESCH, R. E. 1957 *J. Fluid Mech.* **3**, 289–303.

GARCIA, R. U. 1956 *Tellus*, **8**, 82–93.

HELMHOLTZ, H. 1868 *Monatsbericht, Königl. Akad. Wiss., Berlin*, pp. 215–28.

LESSEN, M. 1950 *Nat. Adv. Comm. Aero., Wash., Tech. Rep.* no. 979.

LESSEN, M. & FOX, J. A. 1955 *50 Jahre Grenzschichtforschung*, pp. 122–6. Braunschweig: Friedr. Vieweg.

LIN, C. C. 1955 *The theory of Hydrodynamic Stability*. Cambridge University Press.

MICHALKE, A. 1963 *AFOSR Tech. Note* no. 2; Contract AF 61 (052)–412. 31 May 1963. Also: *Ing. Arch.* **33**, 264–76 (1964).

RAYLEIGH, LORD 1880 *Sci. Papers*, **1**, pp. 474–87. Cambridge University Press.

SATO, H. 1960 *J. Fluid Mech.* **7**, 53–80.

SCHADE, H. & MICHALKE, A. 1962 *Z. Flugwiss.* **10**, 147–54; also *AFOSR Tech. Note* no. 3191.

STUART, J. T. 1961 *Adv. Aero. Sci.* 3–4, 121–42.

TATSUMI, T. & GOTOH, K. 1960 *J. Fluid Mech.* **7**, 433–41.

TATSUMI, T. & KAKUTANI, T. 1958 *J. Fluid Mech.* **4**, 261–75.

TOLLMIEN, W. 1935 *Nachr. Ges. Wiss. Göttingen, Math. Phys. Klasse, Fachgruppe* I, pp. 79–114.

WATSON, J. 1960 *J. Fluid Mech.* **9**, 371–89.

WILLE, R. 1963 *AFOSR Tech. Rep.* Contract AF 61 (052)-412, 30 June 1963.